SEMARAK ILMU PUBLISHING

Journal of Advanced Research in Numerical Heat Transfer

Journal homepage:
https://semarakilmu.com.my/journals/index.php/arnht/index
ISSN: 2735-0142

Computational Fluid Dynamics (CFD) Validation and Investigation the Effect of Piston Bowl Geometries Performance on Port Fuel Injection-Homogeneous Charge Compression Ignition (PFI-HCCI) Engines

Nik Muhammad Hafiz Nik Ab Rashid[1,2,*], Abdul Aziz Hairuddin[1], Khairil Anas Md Rezali[1], Siti Ujila Masuri[1], Al Anbagi Muntasser Abdulabbas Mossa[1], Jamiluddin Jaafar[3], Deni Fajar Fitriyana[4]

[1] Department of Mechanical and Manufacturing Engineering, Universiti Putra Malaysia, 43400, Serdang, Selangor, Malaysia
[2] Centre of Excellence for Technology and Engineering (CREaTE), Jabatan Kerja Raya Malaysia, 78000 Alor Gajah, Melaka, Malaysia
[3] Faculty of Mechanical and Manufacturing Engineering, Universiti Tun Hussein Onn Malaysia, Parit Raja 86400 Batu Pahat, Johor. Malaysia
[4] Department of Mechanical Engineering, Faculty of Engineering Universitas Negeri Semarang,Kampus Sekaran, Semarang 50229, Indonesia

ARTICLE INFO

Article history:
Received 25 December2023
Received in revised form 26 January 2024
Accepted 28 Februrary 2024
Available online 30 March 2024

Keywords:
HCCI; Diesel; Piston Bowl; Port Fuel Injection; Computational Fluid Dynamics; Internal Combustion Engine

ABSTRACT

Homogeneous charge compression ignition (HCCI) is an advanced combustion strategy proposed to provide higher efficiency and lower emissions than conventional compression ignition. Nevertheless, the operation of HCCI engines still presents formidable challenges. Preparing homogeneous mixtures and controlling the combustion phase are crucial challenges in the context of engine performance. Piston bowl geometry significantly enhances the process by improving the flow and facilitating air-fuel mixing for combustion. On that note, this study utilised the CFD simulation methods to analyse HCCI combustion in port fuel injection (PFI) mode and evaluate the effect of piston bowl geometries on engine performance. For this purpose, the CFD simulation result for a single-cylinder, four-stroke YANMAR diesel engine was validated with experimental data. The different piston bowl geometries with the same volume, compression, and equivalence ratio were then investigated numerically. The validation result of the CFD simulation offers enough confidence to continue the study with different piston bowl geometries. The results attained from the Direct Injection (DI) engine piston bowl application demonstrate a minor change in in-cylinder pressure and heat release rate. The piston bowl design employed in a Port Fuel Injection engine application exhibited different combustion phases while demonstrating similarity in attaining in-cylinder pressure. The findings for swirl induce piston bowl design indicate an enhancement of in-cylinder pressure for the Spiral Crown geometry model, reaching 9.42 MPa. The results of the study demonstrated that the piston bowl's design affected the performance of an HCCI engine.

1. Introduction

Hydrocarbon fuels have been the most popular transportation and power generation option for more than a century. The expansion of the automobile industry and the increase in the number of

* *Corresponding author.*
E-mail address: nikmhafiz@jkr.gov.my (Nik Muhammad Hafiz Nik Ab Rashid)

https://doi.org/10.37934/arnht.18.1.3048

vehicles have increased the risk of fossil fuel depletion and pushed exhaust gas emissions to a critical level [1-5]. To achieve this purpose, numerous combustion approaches have been studied to fulfil future requirements for clean and efficient combustion engines. Most of the current strategies fall within low-temperature combustion (LTC). In this regard, the homogeneous charge compression ignition (HCCI) combustion mode has the potential [6-10].

The HCCI engine is regarded as a promising technology in engine research, owing to its ability to enhance thermal efficiency while maintaining low emissions. The key objectives of HCCI combustion are to reduce the flame temperature and improve the charge homogeneity through adequate air and fuel mixing. It may be implemented by altering either Spark Ignition (SI) or Compression Ignition (CI) engines [11]. Significant progress has been made in the three primary research fields of HCCI: fundamental theory, gasoline-fuelled HCCI combustion and diesel-fuelled HCCI combustion [12]. Regarding the fuels, gasoline has high volatility; thus, evaporation is rapid, and a premixed charge can be obtained using port fuel injection. But the gasoline is resistant to auto-ignition; it becomes difficult to achieve combustion at low-load conditions [13,14]. On the other hand, diesel fuel has superior auto-ignition qualities since it exhibits notable cool-combustion chemistry, leading to rapid auto-ignition once compression temperatures exceed the ignition temperature of 800K [15].

Nevertheless, the effective implementation of HCCI engines for diesel fuel encounters significant obstacles, particularly in controlling combustion phasing and extending the operating range [12]. Preparing a homogeneous mixture in diesel is challenging due to the lower volatility, higher viscosity, and lower resistance to auto-ignition. The process requires elevated temperatures before vaporization occurs in order to form a premixed homogeneous charge. The essential factor needed to achieve diesel HCCI combustion is the mixture control, including charge components, temperature control throughout the combustion process, and high pre-ignition mixing rates [14]. The impact of piston bowl geometry on an engine's flow, turbulence, mixing, and combustion has been extensively ascertained in the literature [16-23]. Improvements in fuel-air mixing within the cylinder have the potential to greatly improve combustion, thereby increasing engine performance [24].

The primary factors influencing the gas flow within the cylinder are the fluid's swirl and turbulent kinetic energy, which in turn affect the flame propagation within the cylinder [25]. Researchers have shown significant interest in the combustion chamber design of diesel engines over the past decade, as it offers various methods to enhance the airflow within the engine's cylinders. The study conducted by Rakopoulos *et al.,* investigated the effects of piston bowl geometry and speed on a diesel-powered engine [26]. According to their findings, the relationship between combustion chamber geometry, fuel injection, and gas flow is essential for defining combustion characteristics. A key objective in designing the combustion bowl then is to ensure that the mixing of fuel and air is adequate to mitigate the adverse effects of fuel-rich regions and allow the engine to meet its performance targets. In light-duty direct injection (DI) diesel engines, combustion chamber geometry influences the complex interactions between swirl and squish flows, spray-wall interactions, and late-cycle mixing [27]. There are three principal classifications of pistons which are dome, flat, and bowl. The most common pistons in HCCI engines are bowl types, dome-shaped pistons, and specialised pistons, each of which offers distinct advantages and disadvantages [28]. This circumstance has inspired researchers to investigate the beneficial impact of piston bowls on HCCI combustion engines in greater depth.

The complex structure of the internal combustion engine has limited the ability to conduct experimental research on the geometry of the piston bowl. The study will incur to be costly and time-consuming. Therefore, CFD simulation has become a valuable tool for investigating and developing control strategies for the engine due to its higher flexibility and lower cost compared to the experimental approach [29]. The latest Computer Fluid Dynamic (CFD) software employs a highly

efficient coupling of detailed chemical kinetics, liquid fuel spray and turbulent gas dynamics in order to simulate combustion processes occurring in an internal combustion engine. However, the majority studies on the piston geometry conducted in the CFD approach have focused on CI engines [20,30,31]. Regarding the HCCI- PFI engine, most studies have yet to be conducted on the piston bowl geometry design [32-35]. Researching HCCI-PFI is essential because it enables adequate time for thorough air and fuel mixing, leading to an entirely homogeneous mixture and improved performance. In order to achieve this objective, the computational fluid dynamics (CFD) simulation result for a YANMAR diesel engine with a single-cylinder and four-stroke configuration was compared and validated against experimental data. Numerical investigations were subsequently conducted to examine different piston bowl geometries possessing identical volume, compression, and equivalence ratios. The results were analysed based on thermodynamic performance, specifically on the in-cylinder pressure and the heat release rate.

2. Methodology

The research was carried out through experimental and CFD simulation. The experimental method has been used in a modified single-chamber Direct Injection Compression Ignition (DICI) engine to demonstrate the HCCI combustion and play a significant role in validation purposes. On the other hand, the CFD simulation approach has been employed to investigate the effect of different piston bowl geometries on engine performance.

2.1 Experimental Setup

The experiments were conducted on Yanmar L48N, a four-stroke single-cylinder, air-cooled, compression ignition (CI) diesel engine. The detailed specification is listed in Table 1. Researchers frequently employ this particular engine type due to its straight forward mechanism, which facilitates easy modification for conducting fundamental study [36,37]. Preheating system is one of the control techniques to regulate the intake air temperature to switch the engine combustion to HCCI mode. For this case, an external air heater, a STANLEY-forced air heater, and Watlow heater 988A-20CC-CCRR were used to accommodate the heater pipe and control the intake manifold temperature. Besides that, a high-pressure 140-bar Volkswagen injector was connected to the same fuel pipeline with the current Diesel Injector (DI) and was used as Port Fuel Injection (PFI) combustion system. This technique, therefore, enables the PFI injector mechanism to work simultaneously with the DI injector (HCCI-DI) with the aid of an electronic computer unit (ECU) [38]. The detailed parameters for engine set-up are provided in Table 2.

Various sensors and actuators were connected to the experimental engine, including an eddy current dynamometer, airflow meter, exhaust gas analyser, thermocouples, lambda sensor, and in-cylinder pressure sensor. An eddy current Tops Landtop dynamometer model, GFA174A-5, was used in the study. The dynamometer was then connected to its data logger and software to display and record speed, torque, and load data. Lambda (λ) sensor with a digital display uses an MTX-L digital air-fuel ratio gauge, and a Bosch heated wideband oxygen sensor located inside the exhaust gas pipe. The data of the air/fuel ratio was continuously obtained by the sensor at different engine loads during the engine operation. This study used two k-type thermocouples to monitor the engine and exhaust temperature; one was installed on the engine body close to the rotary blade, and another was installed next to the exhaust port. To complete the monitoring system, a pressure transducer Optrand model D5229-R41 was used to measure in-cylinder pressure. The sensor can measure pressure at a range from 0 to 5000 psi with a sensitivity of 0.84 mV/psi at 200°C. The transducer was

connected to its own DAQ system to amplify the signal before it was read and sent to the computer. The schematic diagram of the engine setup for this study is shown in Fig. **1**.

Table 1
Technical details of the YANMAR engine

Engine	YANMAR, L48N, single-cylinder
Cylinder bore	70 mm
Stroke length	58 mm
Compression ratio	20.1:1
Cooling system	Air
Fuel	Diesel
Exhaust valve close	385° CA
Intake valve open	335° CA
Intake valve close	559° CA

Table 2
Experimental set-up parameters

Speed	2700 RPM
Injection system	DI and PFI (modified)
Equivalence ratio	0.42
Intake temperature	343.5 K
Engine load	10 %
Fuel injection pressure	140 bar

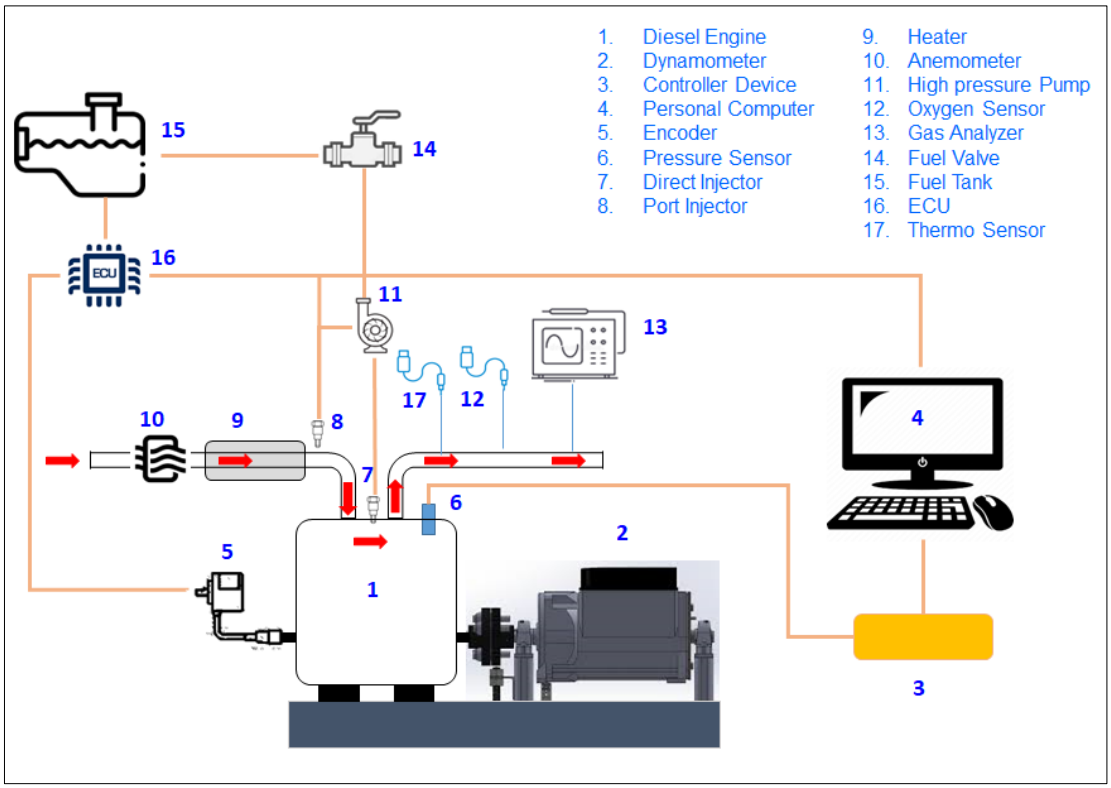

Fig. 1. Schematic diagram for HCCI engine set-up for the study

2.2 Simulation Setup

ANSYS Forte 2021 R2 (ANSYS Forte), a CFD software for internal combustion engine design applications, was used to model and simulate PFI-HCCI combustion in this study. The main structure

of the thermo-fluids is directed by governing equations based on the conservation law of fluids' physical properties. ANSYS Forte applies a turbulent reacting flow representation in which the Navier-Stokes equations govern the basic fluid dynamics. Model transport equations of mass, momentum, and energy conservation laws are formulated for the compressible and gas-phase flows and represent the turbulent nature of the flow [39].

In this study, a series of CFD simulations was performed to demonstrate HCCI combustion in PFI mode and evaluate piston geometries' effect on engine performance. The simulation was conducted based on experimental works conditions in Table 1. A reduced n-heptane chemistry mechanism surrogates the diesel fuel for the simulation works. The chemistry file is a standard ANSYS Chemkin-Pro chemistry-set file containing 36 species and 74 reactions for a semi-detailed n-heptane model. This mechanism is validated based on fundamental experimental data for diesel engine operating conditions [40]. In addition, this study assumed the adiabatic wall boundary condition and constant temperatures were given to the walls, similar to the engine working conditions. Table 3 provides the set-up of initial conditions for this CFD study.

Table 3
Initial and boundary condition for CFD model

Cylinder head temperature	425K
Liner temperature	375K
Piston temperature	525K
Initial pressure	1 Bar
Fuel	n-heptene
Injection parameters	
Fuel mass	0.0057g
Nozzle size (diameter)	0.0055 cm

In addition to the original YANMAR L48N piston geometry, which serves as the baseline model, this study aimed to investigate the effects of piston bowl geometry, focusing on three specific design characteristics. This consideration was made subsequent to a thorough evaluation of design requirements and performance, based on the previous studies. The first character of consideration pertains to the piston bowl design derived from the original shape for DI engine application, and the second revolves around a bowl design used for the PFI engine. Lastly, the third character encompasses a bowl design that can generate a substantial level of swirl, thereby facilitating the optimal air-fuel mixing for the combustion process. The models were chosen based on their performance on spark ignition (SI) and compression ignition (CI) engines by previous researchers and are presently being investigated in homogeneous charge compression ignition (HCCI) engines [41-43]. Fig. **2** depicts the domain of the engine components involved in the computational fluid dynamics (CFD) simulation. On the other hand, Fig. **3** illustrates the cut plane of piston bowl with the engine squish, which is utilised for this study.

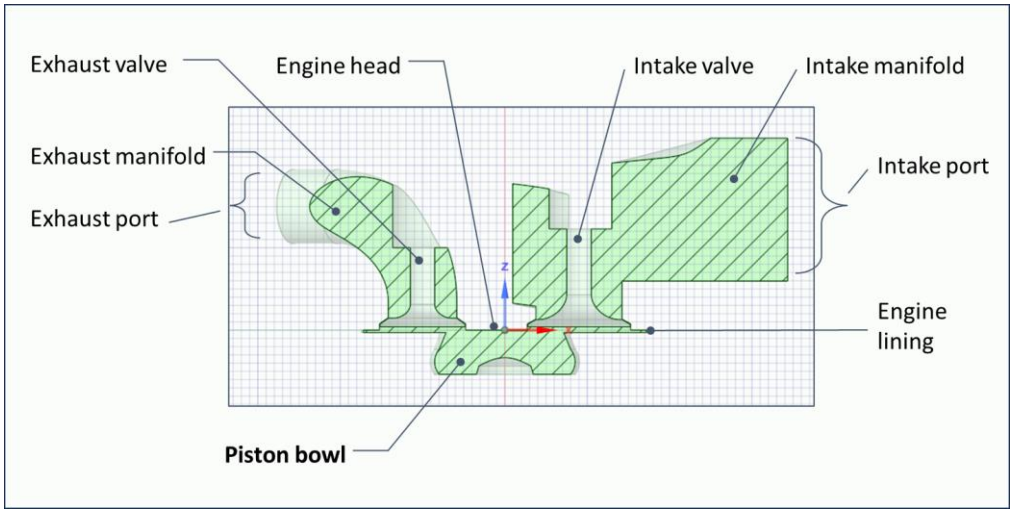

Fig. 2. The engine components domain for CFD simulations study

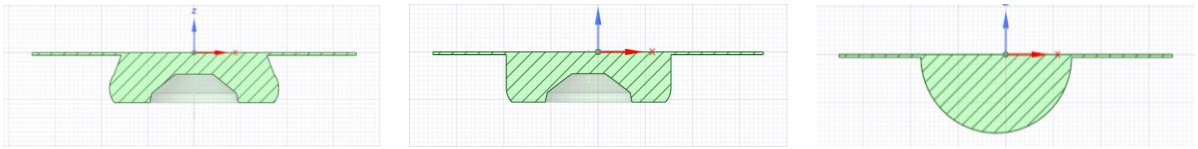

a. DI engine application piston crown

b. PFI engine application piston crown

c. Induce swirl piston crown

Fig. 3. Cut plane of piston bowl geometries with engine squish

2.3 Fluid Continuity Equation

The Fluid Continuity Equation is a fundamental principle in computational fluid dynamics (CFD) and plays a crucial role in simulations within ANSYS Forte. It expresses the principle of mass conservation. It is critical for maintaining mass conservation, linking pressure and velocity fields, and analysing transient and mass transfer phenomena. In this study, the gas-phase working fluids in CFD combustion are modelled as a mixture of individual gas species or components. This composition changes during the engine cycle due to molecular diffusion, flow convection, turbulent transport, interactions with fuel sprays, and combustion. The summation of the equation over all species gives the continuity equation for the total gas-phase fluid as Eq. **Error! Reference source not found.**.

$$\frac{\partial \bar{\rho}}{\partial t} + \nabla \cdot (\bar{\rho}\widetilde{\boldsymbol{u}}) = \dot{\bar{\rho}}^{s} \tag{1}$$

where ρ is density, $\widetilde{\boldsymbol{u}}$ the flow velocity vector and $\dot{\bar{\rho}}^{S}$ is the source term due to spray evaporation.

2.4 Momentum Conservation Equation

The Momentum Conservation Equation is essential for simulating various fluid flow scenarios by governing the motion of fluids. The equation allows us to predict pressure force, convection, turbulent transport, viscous stress, liquid sprays, and body force. For ANSYS Forte, the equation is considered as follow:

$$\frac{\partial \bar{\rho}\widetilde{\boldsymbol{u}}}{\partial t} + \nabla(\bar{\rho}\widetilde{\boldsymbol{u}}\widetilde{\boldsymbol{u}}) = -\nabla\bar{p} + \nabla\cdot\bar{\boldsymbol{\sigma}} - \nabla\cdot\boldsymbol{\Gamma} + \overline{\boldsymbol{F}}^{\boldsymbol{S}} + \overline{\boldsymbol{\rho}}\,\overline{\boldsymbol{g}} \tag{2}$$

where p is the pressure, $\boldsymbol{F^S}$ is the rate of momentum gain per unit volume due to the spray, $\boldsymbol{g}$ is the specific body force, $\boldsymbol{\sigma}$ is the viscous shear stress, and $\boldsymbol{\Gamma}$ is the stress that accounts for the effects of ensemble-averaging of the nonlinear convection.

2.5 Energy Conservation Equation

According to the First Law of Thermodynamics, the change in internal energy must be balanced by the pressure work and heat transfer. The energy conservation equation is used in this study to understand heat transfer, temperature changes, and the interplay of thermal effects with fluid flow and structural behaviour. For flow issues associated with internal combustion engines, the effects of turbulent transport, convection, turbulent dissipation, sprays, chemical reactions, and enthalpy diffusion of a multicomponent flow must also be considered. The internal energy transport given in Eq. **Error! Reference source not found.** as follows:

$$\frac{\partial \bar{\rho}\tilde{I}}{\partial t} + \nabla\cdot(\bar{\rho}\widetilde{\boldsymbol{u}}\tilde{I}) = -\bar{p}\nabla\cdot\widetilde{\boldsymbol{u}} - \nabla\cdot\bar{\boldsymbol{J}} - \nabla\cdot\boldsymbol{H} + \bar{\rho}\bar{\varepsilon} + \dot{\bar{Q}}^{C} + \dot{\bar{Q}}^{S} - \dot{\bar{Q}}_{rad} \tag{3}$$

where I is the specific internal energy, $\boldsymbol{J}$ is the heat flux vector accounting for contributions due to heat conduction and enthalpy diffusion, $\bar{\varepsilon}$ is the dissipation rate of the turbulent kinetic energy, $\dot{\bar{Q}}^{C}$ and $\dot{\bar{Q}}^{S}$ are the rate of the turbulent kinetic energy due to chemical heat release and spray interactions, $\boldsymbol{H}$ accounts for the effects of ensemble-averaging or filtering of the convection, and $\dot{\bar{Q}}_{rad}$ is the radiative heat loss.

2.6 Gas-phase Mixture Equation of State

For the gas-phase mixture, the Equation of State relates to the thermodynamic properties of the gas mixture's temperature, pressure, volume, and composition. It is used to calculate essential thermodynamic properties, tackle compressible flow problems, model combustion processes, and gain deeper insights into the complex behaviour of flows. The ideal gas law applies in ANSYS Forte, assuming the mixing gas components follow the Dalton model and be defined as Eq. **Error! Reference source not found.** :

$$\bar{p} = R_u\bar{T}\sum_k\left(\frac{\bar{\rho}_k}{W_k}\right) \tag{4}$$

where R_u is the universal gas constant, and W_k is the molecular weight of species k .

The internal energy of an ideal gas is only a function of temperature. The specific internal energy of the gas mixture ($\tilde{I}$) is a mass average of the specific internal energy of individual components ($\tilde{I}_k$), $\bar{y}_k$ is the mass fraction of species k, which are tabulated against temperature:

$$\tilde{I}(\bar{T}) = \sum_k \bar{y}_k \tilde{I}_k(\bar{T}) \tag{5}$$

2.7 Reynolds-Averaged-Navier-Stokes (RANS)

RANS equations offer a statistical method to simulate the impact of turbulence. The simulation of an HCCI engine involves averaging the complete Navier-Stokes equations over time, resulting in extra terms that account for the Reynolds stresses caused by turbulent fluctuations. Turbulent flow is characterised by a wide range of flow length scales as well as large and irregular flow field fluctuations. The Reynolds-Averaged-Navier-Stokes (RANS) method, used for this study, aims to capture the ensemble average of the flow field from a vast number of flow realisations under similar conditions. Since turbulence affects fluid transport and mixing significantly more than laminar flow, the ensemble average of turbulent transport and mixing is identical to large-scale diffusion. The RANS technique eliminates the need to resolve small-scale structures and fluctuations in individual flow realisations while preserving the main effects of turbulence on averaged flow and combustion characteristics. In the RANS technique, the turbulent viscosity v_t is related to the turbulent kinetic energy $\tilde{k}$ and its dissipation rate $\tilde{\varepsilon}$, and the calculation of turbulent viscosity requires both to be modelled. The advanced version of the $\tilde{k} - \tilde{\varepsilon}$ model is derived from Re-Normalized Group (RNG) theory as given in Eq. **Error! Reference source not found.** and Eq. **Error! Reference source not found.** [44].

$$\partial \frac{\bar{\rho}\tilde{k}}{\partial t} + \nabla \cdot \left(\bar{\rho}\tilde{\boldsymbol{u}}\tilde{k}\right) = -\frac{2}{3}\bar{\rho}\tilde{k}\nabla \cdot \tilde{\boldsymbol{u}} + (\bar{\boldsymbol{\sigma}} - \boldsymbol{\Gamma}) : \nabla\tilde{\boldsymbol{u}} + \nabla \cdot \left[\frac{(\mu+\mu_T)}{Pr_k}\nabla\tilde{k}\right] - \bar{\rho}\tilde{\varepsilon} + \dot{\bar{W}}^S \tag{6}$$

and

$$\frac{\partial\bar{\rho}\tilde{\varepsilon}}{\partial t} + \nabla \cdot (\bar{\rho}\tilde{\boldsymbol{u}}\tilde{\varepsilon}) = -\left(\frac{2}{3}c_{\varepsilon 1} - c_{\varepsilon 3}\right)\bar{\rho}\tilde{\varepsilon}\nabla\tilde{\boldsymbol{u}} + \nabla.\left[\frac{(v+v_T)}{Pr_\varepsilon}\nabla\tilde{\varepsilon}\right] + \frac{\tilde{\varepsilon}}{\tilde{k}}\left[c_{\varepsilon 1}(\boldsymbol{\sigma} - \boldsymbol{\Gamma}) : \nabla\tilde{\boldsymbol{u}} - c_{\varepsilon 2}\bar{\rho}\tilde{\varepsilon} + c_s\dot{\bar{W}}^S\right] - \bar{\rho}R \tag{7}$$

in these equations, $Pr_k, Pr_\varepsilon, c_{\varepsilon 1}, c_{\varepsilon 2}, c_{\varepsilon 3}$ are model constants.

2.8 Chemical Kinetics Formulation

ANSYS Forte embedded Chemkin-Pro solver that can incorporate more extensive and accurate fuel models into a simulation. The Chemical Kinetics formulation in ANSYS Forte plays a vital role in simulating reacting flow problems, where chemical reactions occur within the fluid mixture. The Chemkin-Pro solver is utilised for chemical kinetic simulation, utilising unique and exclusive methods to achieve impressive calculation speeds. On that note, the Dynamic Cell Clustering application in the Chemkin-Pro leverages an advanced algorithm to group cells with similar kinetic conditions and eliminate duplicate calculations. Simultaneously, Dynamic Adaptive Chemistry will immediately and automatically lower the kinetics at each time step. Regarding the chemical kinetic mechanism, a simplified reduced n-heptane (nc7h16) mechanism was used in this study as a surrogate to diesel fuel. The chemistry file is a standard ANSYS Chemkin-Pro chemistry-set file, Diesel_1comp_35sp.cks file with 36 species and 74 reactions.

Chemical kinetic mechanisms can accurately describe the chemical reactions that occur in combustion simulations. These mechanisms define the reaction paths and the associated reaction rates that lead to the change in species concentrations. Consequently, the generic form in Eq. **Error! Reference source not found.** can represent reversible or irreversible reactions involving chemical species in detailed chemical kinetic mechanisms [45].

$$\sum_{k=1}^{K} v'_{ki}\chi_k \Leftrightarrow \sum_{k=1}^{K} v''_{ki}\chi_{k(i=1,\ldots,i).} \tag{8}$$

whereby, the production rate of the k^{th} species in the i^{th} reaction can be written as

$$\dot{\omega}_{ki} = (v''_{ki} - v'_{ki})q_i(k = 1, \ldots, K) \tag{9}$$

where q_i is the rate progress of rection i.

The summation of $\dot{\omega}_{ki}$ over all the reactions gives the chemical source term $\dot{\rho}_k^c$ in the species continuity equation as follow:

$$\dot{\rho}_k^c = W_k \sum_{i=1}^{I} \dot{\omega}_{ki} \tag{10}$$

Therefore, the chemical heat release term in the energy equation is denoted by Eq.**Error! Reference source not found.** as follow:

$$\dot{Q}_c = -\sum_{i=1}^{I} Q_i\, q_i = \sum_{i=1}^{I}\sum_{k=1}^{K}(v''_{ki} - v'_{ki})\left(\Delta h_f^0\right)_k q_i \tag{11}$$

where Q_i is heat of reaction of reaction i at absolute zero and $\left(\Delta h_f^0\right)_k$ is the heat of formation of species at absolute zero.

3. Results and Discussion

3.1 Grid Independence Study

The Ansys Forte software utilises a real-time cartesian volume mesh generation technique in conjunction with an immersed boundary approach. The automatic mesh generation at each piston position depends on defined mesh-size criteria and specified mesh refinement settings. The Global Mesh Size sets the overall background mesh size, which is used everywhere when a mesh refinement is not defined. On the other hand, mesh refinement is utilised to resolve both surfaces and regions within the computational geometry where it has been specified. Moreover, Ansys Forte features an adaptive mesh solution that enables mesh refinement based on specific variables such as velocity and temperature [39]. All these mesh refinement options are activated at different periods and sizes according to needs. A smaller mesh size usually would yield a more accurate result. Nevertheless, there is a disadvantage: smaller mesh sizes demand more computational time and power. This consideration is essential as time and power resources are limited.

Mesh-sensitivity study has been conducted using four different grid resolutions with the same boundary and initial conditions. On that note, the global mesh sizes of 0.2 cm and 0.3 cm for cold flow simulation have been tested with and without refining. According to

Table **4**, there were four types of mesh refinement had been employed to this study to enhance accuracy and capture essential flow features. Specifically, the surface refinement technique focused on the wall and moving components. Point refinement was utilised in the vicinity of the port fuel

injection (PFI) area. The solution adaptive mesh (SAM) refinement strategy enhanced resolution in regions characterised by specific velocity and temperature conditions. The secondary volume refinement was concentrated in the squish area during the compression stroke near the top dead centre (TDC). The global mesh size of 0.3 cm underwent refinement to reach a size of 0.0375 cm, corresponding with the specified location and crank angle settings during the simulation. Fig. **4** illustrates the condition of the mesh size at 720 CA° and its comparison with the mesh size that has not undergone mesh refinement.

The findings depicted in Fig. **5** indicate that the mesh sizes of 0.3 cm and 0.2 cm, when used without refinement, were inadequate for the computational fluid dynamics (CFD) simulation. Conversely, the exact mesh sizes exhibited contrasting results when employed with refinement. The details of the four mesh types and the corresponding computational runtime are shown in

Table 5. Taken together all these results, the mesh size of 0.3cm with refinement yielded the optimum accuracy and computational performance, therefore, was used in the subsequent simulations.

Mesh size with refinement Mesh size without refinement

Fig. 4. Comparison of mesh size by employing mesh refinement method

Table 4
Mesh refinement type, location and activation time for CFD simulation

Type	Refinement name	Location/ variable	Size Fraction Of global size	Active time	Size when active Base 0.3 global size (cm)
Surface refinement	Wall	All walls domain	1/2	All time	0.15
	Open boundaries	Intake & Exh port	1/2	All time	0.15
	Valve stems	Intake & Exh stems	1/2	All time	0.15
	Valve seats	Valve seats	1/4	All time	0.075
	Squish 1 & 2	Squish area	1/4	340°CA~380°CA and 690°CA~790°CA	0.075
	Intake manifold	Intake manifold	1/4	380°CA~500°CA	0.075
Point refinement	Injector	Intake manifold	1/4	465°CA~515°CA	0.075
Solution adaptive mesh	SAM-Temp	Temperature	1/4	680°CA~800°CA	0.075
	SAM-Velocity	Velocity magnitude	1/2	All time	0.15
	SAM-Velocity-Manifold	Velocity magnitude	1/2	380°CA~500°CA	0.15
Secondary Volume	Squish 1 & 2	Squish area	1/8	350°CA~370°CA and 700°CA~740°CA	0.0375

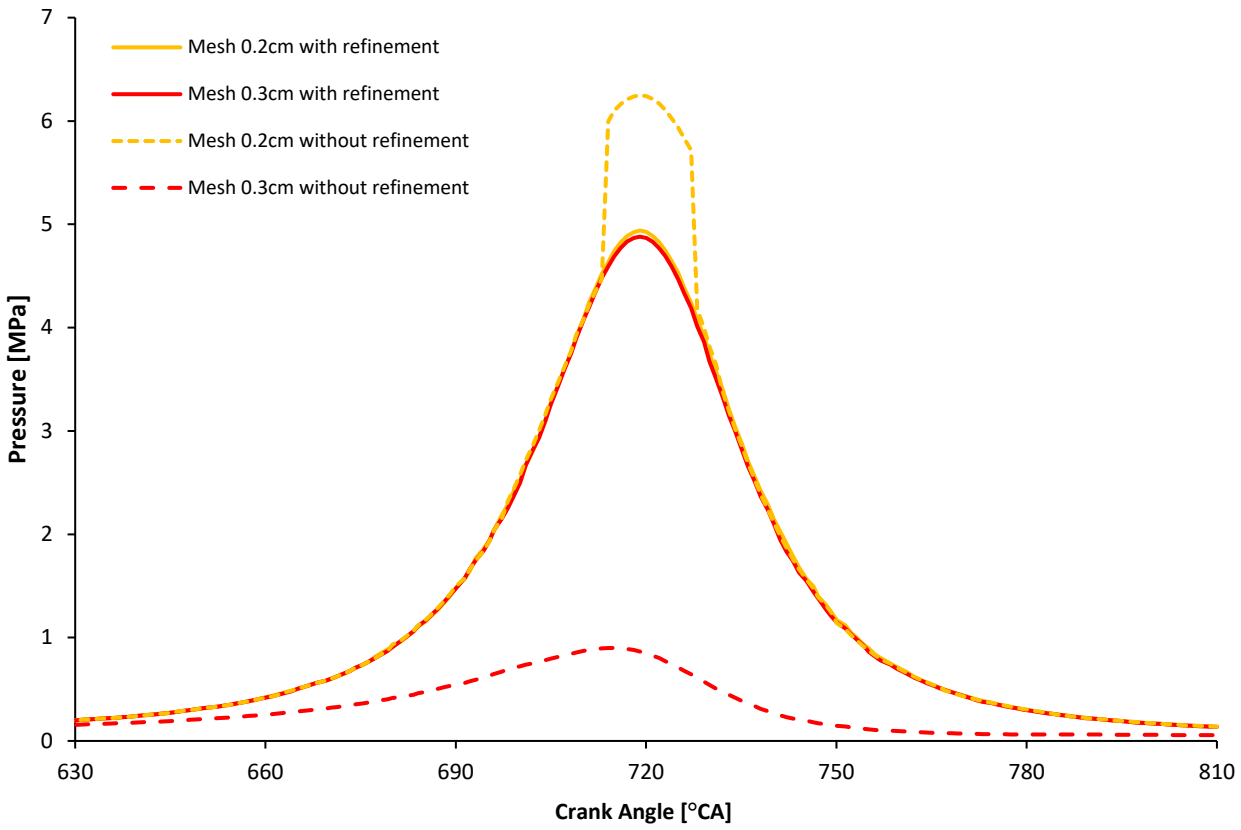

Fig. 5. In-cylinder pressure obtained for cold-flow simulation with different mesh size and technique

Table 5
Computational mesh details for different mesh size and technique

Global mesh size	Max. numbers of cells	Max. Pressure (MPa)	Storage Requirement (Gbytes)	Runtime (hours)
0.2 Refinement	347,929	4.94	17.30	109.25 hours
0.3 Refinement	148,080	4.88	7.79	36.15 hours
0.2 w/o refinement	52,061	6.25	2.69	41.25 hours
0.3 w/o refinement	41,652	0.90	1.47	20.25 hours

3.2 Model Validation

A validation study was performed to compare the results of computational fluid dynamics (CFD) simulation with experimental data. The study was conducted under controlled conditions, with the piston bowl volume, compression ratio, engine speed, and injected fuel mass kept constant. When conducting CFD simulations, it is essential to acknowledge the constraints and presumptions that may impact the accuracy, reliability, and applicability of the outcomes. Therefore, it is crucial that the input parameters, precisely the initial condition and boundary condition used in the CFD simulation setup, accurately or substantially mirror the conditions in the empirical investigation. Nevertheless, the modelling method is limited by its inherent limitations and necessitates the inclusion of certain assumptions. The simulation results covered the duration between the intake valve opening (IVO) and the exhaust valve closing (EVC), operating at an ambient temperature of 303.5K and an engine speed of 2700 rpm. Given that the simulation was performed under adiabatic conditions, the most complex challenge faced during the simulation was determining the temperatures of the walls. A sensitivity analysis was performed to assess the impact of temperature variations on the wall

temperature of the piston, liner, and engine head. The temperature range explored was between 375K and 550K, with temperature increments of 25K.

Fig. **6** shows in-cylinder pressure and heat release rate for CFD simulation and experimental works. Heat release rate, often called fuel combustion rate, is a method for determining the rate of chemical energy release from a fuel. For experimental works, the average pressure data were obtained from the dynamometer, and the heat release rate was then determined by applying the first law of thermodynamics. The experimental work was carried out with 343.5 K intake temperature and the parameter setup as per shown in Table 1. As shown in Fig. **6**, the CFD simulation result shows good agreement with the experimental data. Based on the findings, the maximum value of in-cylinder pressure demonstrates 1.97 % deviation compared to the experimental profile. The heat release rate, then, exhibited a maximum error of approximately 0.5% However, the timings of the peak heat release rate could be better predicted. The peak pressure and heat release rate are obtained at 3° bTDC for simulation instead of 7° bTDC for the experimental case.

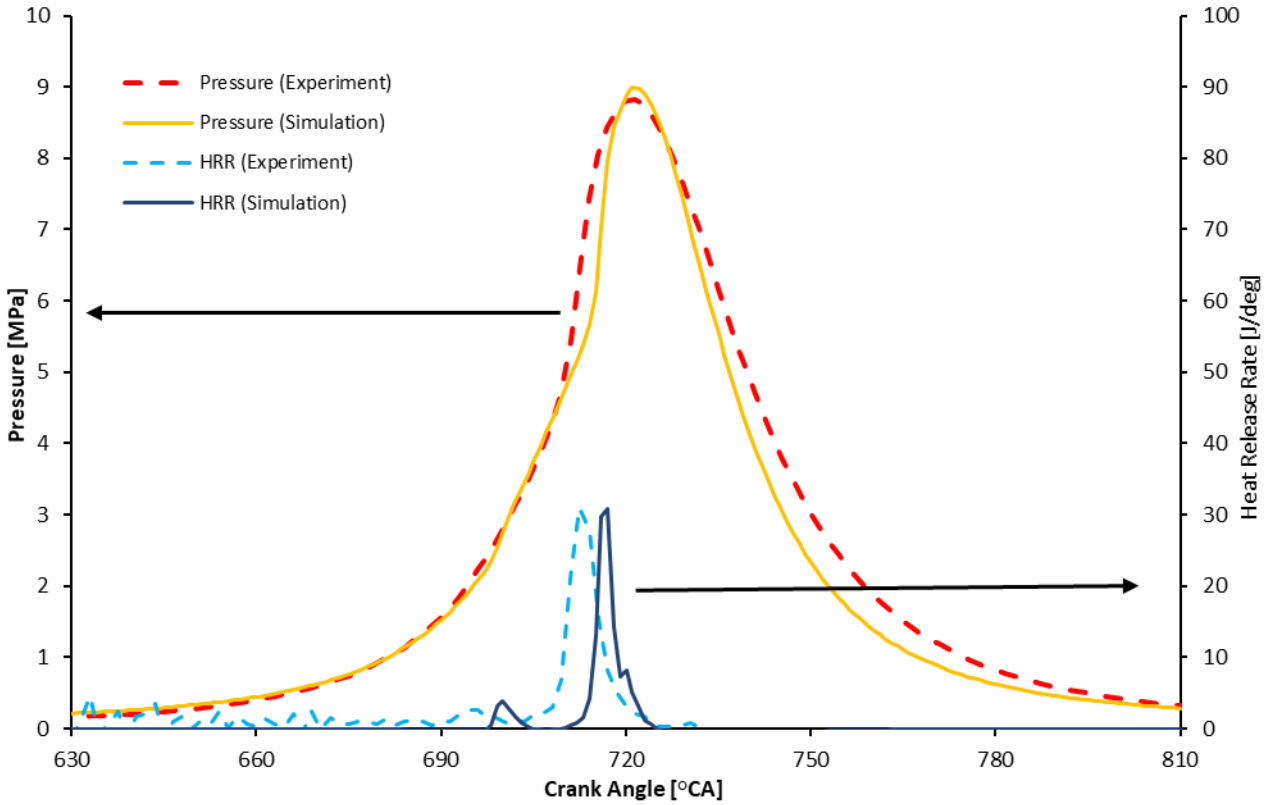

Fig. 6. Comparison of In-cylinder Pressure and Heat Release Rate

Several factors could explain this observation. The discrepancy in in-cylinder pressure and heat release rate between CFD simulation data and experimental results can be attributable to two leading causes. The first is due to the assumptions made for the values of several engine specifications that were unavailable from the manufacturer and difficult to obtain. The second plausible cause for the discrepancy between simulation and experimental results is the assumptions made when developing the model, such as the boundary conditions [46]. Since actual combustion chamber wall and piston surface temperatures could not be measured, values were derived using plausible estimates for

normal operating conditions based on published literature. Notwithstanding these drawbacks, the results provide sufficient confidence for the present study.

3.3 In-Cylinder Pressure and Heat Release Rate in Different Piston Bowl Geometries

For an Internal Combustion Engine (ICE), in-cylinder pressure changes with crank angle due to changes in cylinder volume, combustion, and heat transfer to the cylinder wall. In this respect, cylinder volume and combustion changes contribute the most [25]. On the other hand, the start of combustion can be determined via the heat release rate which rises from negative to positive value, while, the end of combustion is defined as the point where the heat release rate value is zero. However, determining the end of combustion poses a certain degree of difficulty. During this CFD simulation study, the effect of a volume changes on in-cylinder pressure were calculated, and then the information on the combustion rate were derived from precise pressure measurements. Fig. **7** to Fig. **9** present the result of in-cylinder pressure and heat release rate for different piston bowl geometries, as previously characterised and elucidated in Fig. **3**.

3.4 In-cylinder Pressure and Heat Release Rate in DI Engine Application Piston Bowl Design

The outcome results acquired for the design DI engine piston bowl application shown in Fig. **7** demonstrate a minor change for both in-cylinder pressure and heat release rate. The Straight Wall piston bowl geometry exhibits a peak in-cylinder pressure of 9.0 MPa, almost similar as the Baseline model. In contrast, the Hemispherical piston bowl geometry demonstrated a peak in pressure obtained of 8.82 MPa, indicating a reduction of 2.0%. The outcome of this investigation contrasts with the findings of a previous study conducted using the direct injection method [41]. In that study, the peak pressure achieved for the toroidal geometry (baseline) was greater than that for the hemispherical geometry. This phenomenon could be attributed to the fluctuating swirl motion of air produced within the combustion chamber, leading to disparate combustion characteristics [47]. Regarding the heat release rate, the piston bowl geometries for the Baseline, Straight Wall, and Hemispherical models depicted similar combustion phases but varied in the peak of heat release rate. The Straight Wall model achieved the highest peak value of heat release rate at 31.46 J/°CA, while the Baseline and Hemispherical models obtained peak values of 30.83 J/°CA and 26.60 J/°CA, respectively. In general, the DI engine application piston bowl demonstrated a minimal deviation in terms of in-cylinder pressure. The discrepancy can only be triggered for the peak value of heat release rate.

3.5 In-cylinder Pressure and Heat Release Rate in PFI Engine Application Piston Bowl Design

The piston bowl design implemented in the PFI engine application (Fig. **8**) exhibits a distinct outcome compared to the Baseline model. The Exhaust Squish piston bowl design slightly improved the In-cylinder pressure, reaching a peak value of 9.05 MPa. The increment of in-cylinder peak pressure for Exhaust Squish indicated a marginal improvement of less than 1%. Conversely, the Intake Squish piston bowl resulted in a decrease in pressure at 8.78 MPa. The discrepancy in pressure between the exhaust squish and the intake squish can be attributed to the variation in vortex generation and subsequent dissipation. The dissipation of the tumble in the smaller vortex, as it encounters non-planar surfaces on the piston bowl, is a crucial characteristic for fuel distribution within the combustion chamber. However, it also dissolves flow energy, which is beneficial for the development of flames during the combustion process [42,43]. As for the heat release rate, the

results revealed that the combustion occurred at various crank angle positions. The combustion process for the Exhaust Squish piston bowl was observed at the earliest crank angle degree, specifically at 713°CA. Subsequently, the Baseline piston bowl was at 714°CA, while the Intake Squish piston bowl experienced combustion at 715°CA. The combustion characteristics of the piston bowl in the PFI engine application demonstrate minimal alteration in obtaining in-cylinder pressure while exhibiting notable changes in combustion phases.

3.6 In-cylinder Pressure and Heat Release Rate in Swirl Induce Piston Bowl Design

The airflow from the valve to the cylindrical combustion chamber, known as Swirl, is crucial in the combustion process as it improves the mixing rate in a compression ignition engine's chamber [48]. Therefore, this study has fabricated two piston bowl designs corresponding to swirl profiles in combustion chambers. The outcomes of the piston bowl specifically designed to induce the swirl depicted in Fig. **9**, as the results, the Spiral Crown piston geometry exhibited 9.42 MPa of in-cylinder pressure, 5% higher than the Baseline geometry. On the other hand, the Spiral Cylinder geometry obtained 8.97 MPa of in-cylinder pressure, almost a similar value obtained for the Baseline geometry. The geometry design to enhance the swirl during the intake and compression stroke has demonstrated the highest peak pressure due to its ability to improve mixture quality by enhancing airflow movement in the combustion chamber [18,48,49]. The results for heat release rate exhibited different peak values, combustion periods, and the start of combustion. Spiral Crown geometry attained the heat release rate of 32.36 at 716°CA, contra with Spiral Cylinder that attained the heat release rate of 41.55 at 717°CA. The finding from heat release rate indicated that the advanced combustion with a sufficient combustion period resulted in a higher in-cylinder pressure for the combustion.

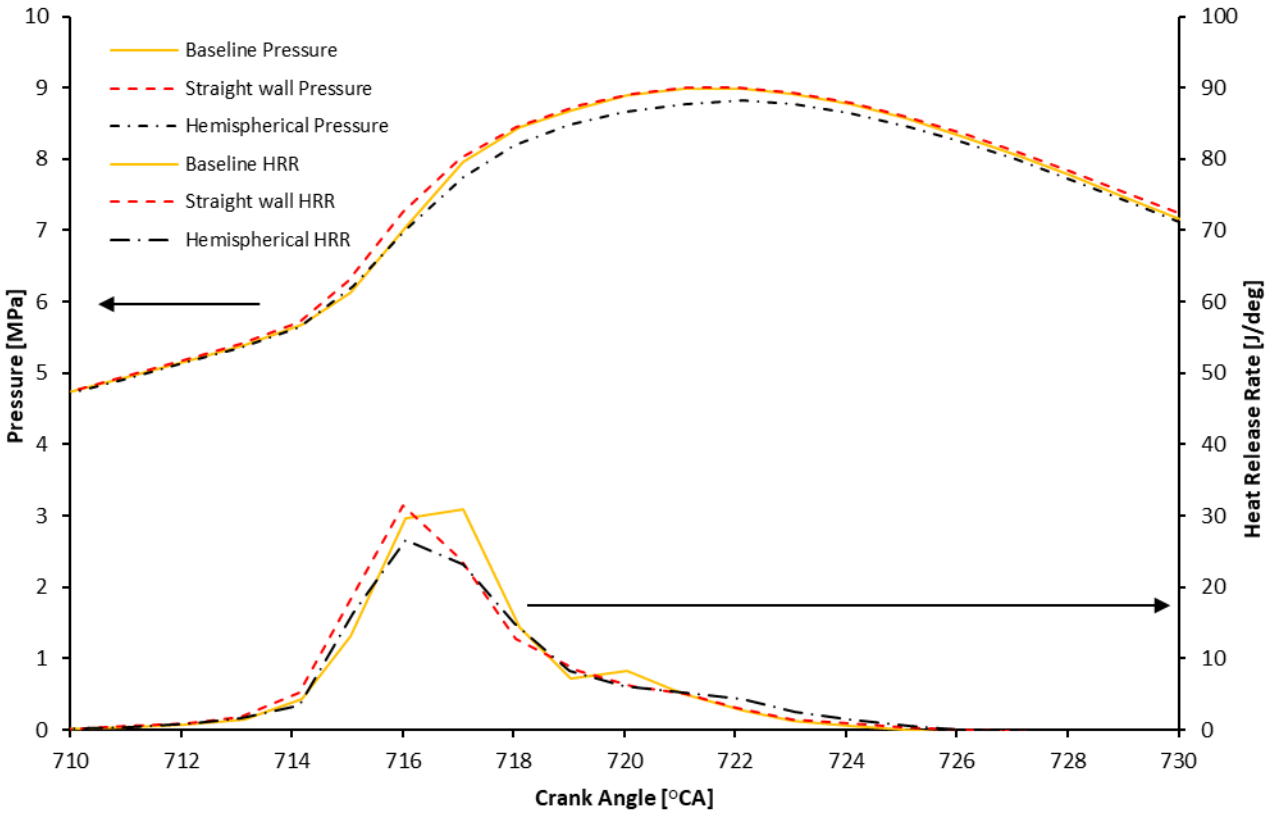

Fig. 7. In-cylinder pressure and heat release rate for DI engine application piston bowl

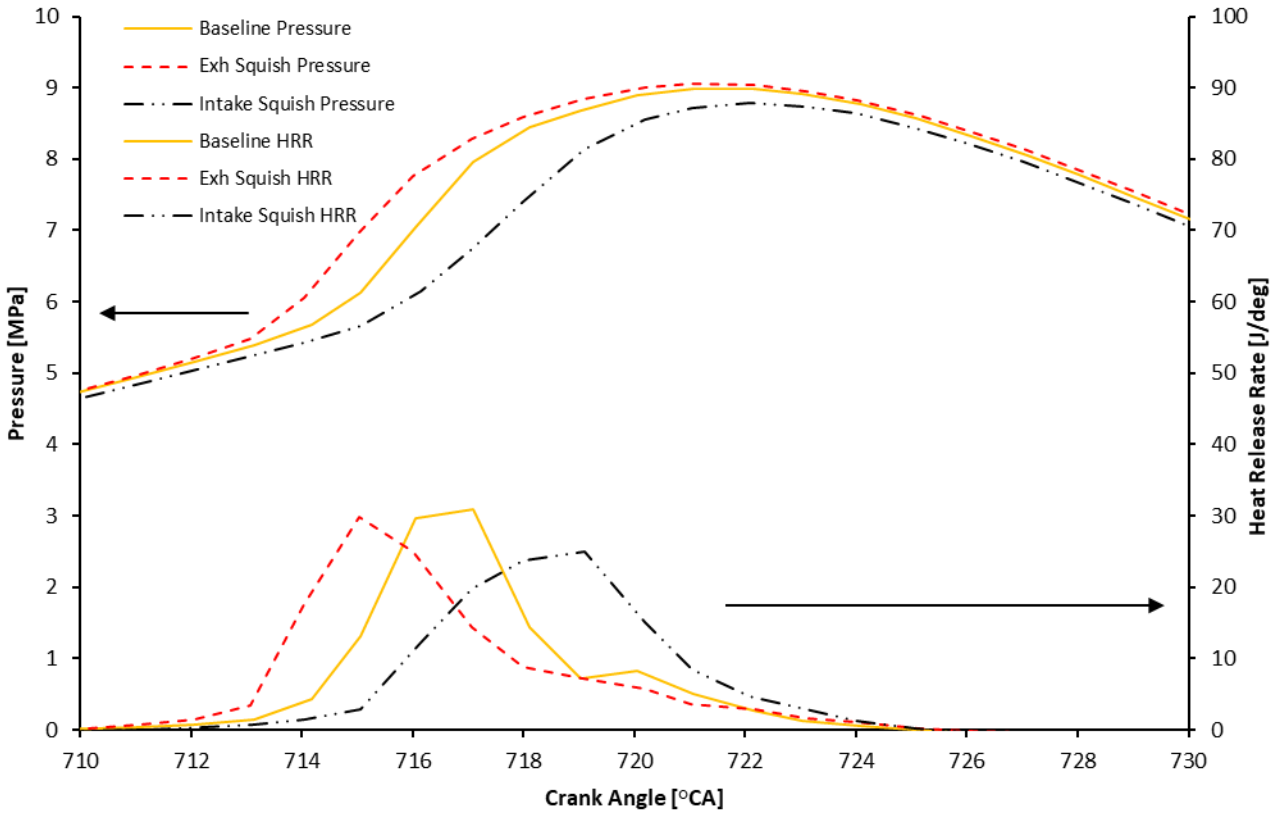

Fig. 8. In-cylinder pressure and heat release rate for PFI engine application piston bowl

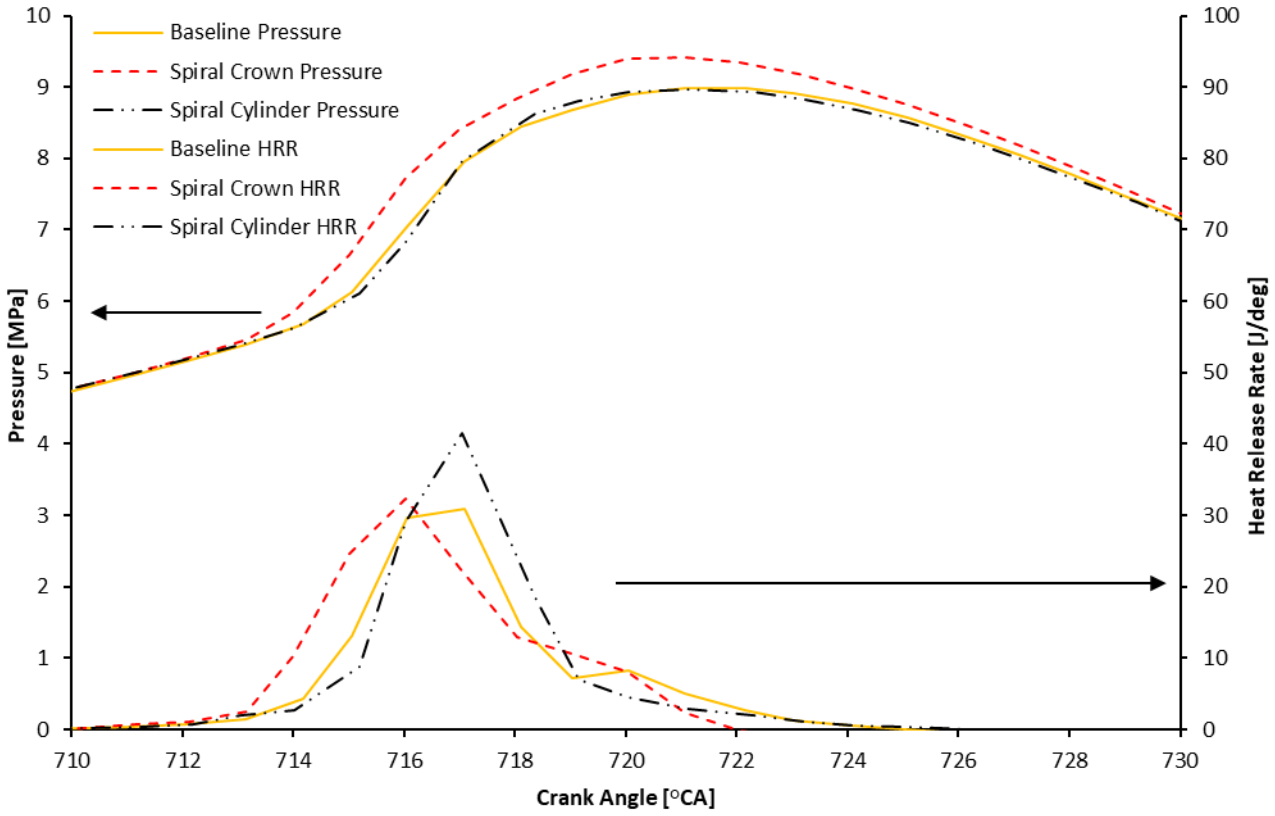

Fig. 9. In-cylinder pressure and heat release rate for swirl induce piston bowl

4. Conclusions

The objectives of this study were to validate the CFD simulation of the PFI-HCCI combustion engine on a modified Yanmar L48N engine and evaluate the effect of piston bowl geometries on the engine performance. Along the comparison study on different piston bowl geometries, the piston bowl volume, compression ratio, engine speed, and injected fuel mass were maintained at a constant level, thereby enabling the results to be purely attributed to the piston bowl geometry. The simulation results covered the period from the intake valve open (IVO) to the exhaust valve close (EVC) at an engine speed of 2700 RPM. The results indicate that:

1) The computational fluid dynamics (CFD) simulation results show a significant degree of agreement with the experimental data. The maximum in-cylinder pressure exhibits a deviation of 1.97% compared to the experimental profile. The heat release rate demonstrated a maximum error of approximately 0.5%.
2) The outcome results acquired for the design DI engine piston bowl application demonstrate a minor change for in-cylinder pressure and heat release rate. The Straight Wall piston bowl design demonstrated a similar value of in-cylinder pressure of 9.0 MPA, while the Hemispherical design indicated a reduction of 2% compared to the Baseline model.
3) The piston bowl design employed in a PFI engine application yielded different combustion phases while demonstrating similarity in attaining in-cylinder pressure. The exhaust Squish geometry model achieved advanced combustion, reaching the peak of heat release rate at 713°CA, followed by the Baseline and Intake Squish geometry models at 714°CA and 715°CA, respectively.
4) The findings for swirl induce piston bowl design indicate an enhancement of in-cylinder pressure for the Spiral Crown geometry model, reaching 9.42 MPa. Nevertheless, the Spiral Cylinder demonstrate a marginal decrease in pressure value. The swirl induced geometry model exhibits the effect of peak heat release rate value, the start of combustion, and the combustion period.
5) The results of the study revealed that piston bowl design could affected performance and combustion control of the HCCI engine, which is a critical part of demonstrating HCCI combustion.

Based on the research findings, it is recommended to develop a piston geometry model using a spiral crown piston bowl. Prior to that, it is advisable to conduct a thorough investigation of piston bowl parameters, including size, diameter, depth, location, and rotational direction.

Acknowledgement

The authors appreciate Universiti Putra Malaysia for research facilities and grants. The study is supported by the GP-IPS research grant from UPM with project code GP-IPS 9706000 and in part by the Malaysia Fundamental Research Grant Scheme (FRGS) with reference code of FRGS/1/2015/TK03/UPM/02/4 under the project code 03-01-15-1629FR and VOT number 5524734.

References

[1] Lyu, Pu, Peirong Slade Wang, Yuanyuan Liu, and Yuanqing Wang. "Review of the studies on emission evaluation approaches for operating vehicles." Journal of Traffic and Transportation Engineering (English Edition) 8, no. 4 (2021): 493-509. https://doi.org/10.1016/j.jtte.2021.07.004

[2] IEA, "Energy Technology Perspectives 2020," Energy Technology Perspectives 2020, IEA, Paris, 2020. https://www.iea.org/reports/energy-technology-perspectives-2020
[3] Zhang, Linling, Ruyin Long, Hong Chen, and Jichao Geng. "A review of China's road traffic carbon emissions." Journal of Cleaner Production 207 (2019): 569-581. https://doi.org/10.1016/j.jclepro.2018.10.003
[4] ACEA, "Car and van CO2 targets: Europe needs a realistic roadmap to reach carbon neutrality," 2022. https://www.acea.auto (accessed Oct. 02, 2022).
[5] Ahmad, Zishan, Mohammad Junaid Khan, and Md Naqui Akhtar. "A Critical Review of Hybrid Electric Vehicles." Journal of Advanced Research in Applied Sciences and Engineering Technology 29, no. 1 (2022): 283-294. https://doi.org/10.37934/araset.29.1.283294
[6] Babagiray, Mustafa, Tolga Kocakulak, Seyed Mohammad Safieddin Ardebili, Hamit Solmaz, Can Çınar, and Ahmet Uyumaz. "Experimental and statistical investigation of different valve lifts on HCCI combustion, performance and exhaust emissions using response surface method." Energy 244 (2022): 123184. https://doi.org/10.1016/j.energy.2022.123184
[7] Tobib, Hasyuzariza M., Hamzah Rostam, Muntasser AA Mossa, A. Aziz Hairuddin, and M. M. Noor. "The performance of an HCCI-DI engine fuelled with palm oil-based biodiesel." In IOP Conference Series: Materials Science and Engineering, vol. 469, no. 1, p. 012079. IOP Publishing, 2019. https://doi.org/10.1088/1757-899X/469/1/012079
[8] Puškár, Michal, and Melichar Kopas. "System based on thermal control of the HCCI technology developed for reduction of the vehicle NOX emissions in order to fulfil the future standard Euro 7." Science of the Total Environment 643 (2018): 674-680. https://doi.org/10.1016/j.scitotenv.2018.06.082
[9] Hasan, M. M., and Md Mustafizur Rahman. "Homogeneous charge compression ignition combustion: Advantages over compression ignition combustion, challenges and solutions." Renewable and Sustainable Energy Reviews 57 (2016): 282-291. https://doi.org/10.1016/j.rser.2015.12.157
[10] Alias, M. S. M., A. A. Hairuddin, M. K. Hassan, and K. A. M. Rezali. "A review of hydrogen addition in an HCCI engine fueled with biofuels." In AIP Conference Proceedings, vol. 2059, no. 1. AIP Publishing, 2019. https://doi.org/10.1063/1.5085988
[11] Gray III, Allen W., and Thomas W. Ryan III. "Homogeneous charge compression ignition (HCCI) of diesel fuel." *SAE transactions* (1997): 1927-1935. https://doi:10.4271/971676
[12] Yao, Mingfa, Zhaolei Zheng, and Haifeng Liu. "Progress and recent trends in homogeneous charge compression ignition (HCCI) engines." Progress in energy and combustion science 35, no. 5 (2009): 398-437. https://doi.org/10.1016/j.pecs.2009.05.001
[13] Liu, Haifeng, Mingfa Yao, Bo Zhang, and Zunqing Zheng. "Effects of inlet pressure and octane numbers on combustion and emissions of a homogeneous charge compression ignition (HCCI) engine." Energy & Fuels 22, no. 4 (2008): 2207-2215. https://doi.org/10.1021/ef800197b
[14] Christensen, Magnus, Anders Hultqvist, and Bengt Johansson. "Demonstrating the multi fuel capability of a homogeneous charge compression ignition engine with variable compression ratio." SAE transactions (1999): 2099-2113. https://doi.org/10.4271/1999-01-3679
[15] Kelly-Zion, Peter L., and John E. Dec. "A computational study of the effect of fuel type on ignition time in homogenous charge compression ignition engines." Proceedings of the Combustion Institute 28, no. 1 (2000): 1187-1194. https://doi.org/10.1016/S0082-0784(00)80329-X
[16] Pastor, José V., Antonio García, Carlos Micó, Felipe Lewiski, Alberto Vassallo, and Francesco Concetto Pesce. "Effect of a novel piston geometry on the combustion process of a light-duty compression ignition engine: An optical analysis." Energy 221 (2021): 119764. https://doi.org/10.1016/j.energy.2021.119764
[17] Benajes, Jesús, Antonio García, José Manuel Pastor, and Javier Monsalve-Serrano. "Effects of piston bowl geometry on Reactivity Controlled Compression Ignition heat transfer and combustion losses at different engine loads." Energy 98 (2016): 64-77. https://doi.org/10.1016/j.energy.2016.01.014
[18] Mittal, Gaurav, Maharshi Subhash, and Manoj Gwalwanshi. "Effect of initial turbulence on combustion with ECFM-3Z model in a CI engine." Materials Today: Proceedings 46 (2021): 11007-11010. https://doi.org/10.1016/j.matpr.2021.02.097
[19] Wang, Xinyan, and Hua Zhao. "Effect of piston shape design on the scavenging performance and mixture preparation in a two-stroke boosted uniflow scavenged direct injection gasoline engine." International Journal of Engine Research 22, no. 5 (2021): 1484-1499. https://doi.org/10.1177/1468087419900072
[20] Rizvi, Ikhtedar Husain, and Rajesh Gupta. "Numerical investigation of injection parameters and piston bowl geometries on emission and thermal performance of DI diesel engine." SN Applied Sciences 3, no. 6 (2021): 626. https://doi.org/10.1007/s42452-021-04633-1

[21] Prabhakaran, P., C. G. Saravanan, R. Vallinayagam, M. Vikneswaran, N. Muthukumaran, and K. Ashok. "Investigation of swirl induced piston on the engine characteristics of a biodiesel fueled diesel engine." fuel 279 (2020): 118503. https://doi.org/10.1016/j.fuel.2020.118503
[22] Adeniyi, Oladapo. "Numerical Investigation on the Effect of Piston Bowl Geometry on Combustion Characteristics of a Heavy-Duty Diesel Engine." Mapta Journal of Mechanical and Industrial Engineering (MJMIE) 3, no. 2 (2019): 9-20. https://doi.org/10.33544/mjmie.v3i2.114
[23] Gulcan, Halil Erdi, and Murat Ciniviz. "Experimental study on the effect of piston bowl geometry on the combustion performance and pollutant emissions of methane-diesel common rail dual-fuel engine." Fuel 345 (2023): 128175. https://doi.org/10.1016/j.fuel.2023.128175
[24] Gafoor, CP Abdul, and Rajesh Gupta. "Numerical investigation of piston bowl geometry and swirl ratio on emission from diesel engines." Energy Conversion and Management 101 (2015): 541-551. https://doi.org/10.1016/j.enconman.2015.06.007
[25] Heywood, John B. Internal combustion engine fundamentals. McGraw-Hill Education, 2018.
[26] Rakopoulos, C. D., G. M. Kosmadakis, and E. G. Pariotis. "Investigation of piston bowl geometry and speed effects in a motored HSDI diesel engine using a CFD against a quasi-dimensional model." Energy conversion and management 51, no. 3 (2010): 470-484. https://doi.org/10.1016/j.enconman.2009.10.010
[27] Zha, Kan, Stephen Busch, Alok Warey, Richard C. Peterson, and Eric Kurtz. "A study of piston geometry effects on late-stage combustion in a light-duty optical diesel engine using combustion image velocimetry." SAE International Journal of Engines 11, no. 6 (2018): 783-804. https://doi.org/10.4271/2018-01-0230
[28] Shaver, Gregory M., J. Christian Gerdes, and Matthew J. Roelle. "Physics-based modeling and control of residual-affected HCCI engines." (2009): 021002. https://doi.org/10.1115/1.3023125.
[29] Zhao, Junliang, Ruomiao Yang, Yuchao Yan, Juan Ou, Zhentao Liu, and Jinlong Liu. Numerical study on the effect of injector nozzle hole number on diesel engine performance under plateau conditions. No. 2023-24-0033. SAE Technical Paper, 2023. https://doi.org/10.4271/2023-24-0033
[30] Rather, Mushtaq Ahmad, and Mohammad Marouf Wani. "A numerical study on the effects of exhaust gas recirculation temperature on controlling combustion and emissions of a diesel engine running on HCCI combustion mode." International Journal of Automotive Science and Technology 2, no. 3 (2018): 17-27. https://doi.org/10.30939/ijastech..451574
[31] Coşkun, Gökhan. "Numerical and experimental investigations of the effects of the second injection timing and alcohol-gasoline fuel blends on combustion and emissions of an HCCI-DI engine." (2018). https://doi.org/10.1016/j.fuel.2018.01.061
[32] Pourfallah, Mohsen, Mahbod Armin, and Ali Akbar Ranjbar. "A numerical study on the effect of thermal and charge stratification on the HCCI natural gas engine." International Journal of Ambient Energy 42, no. 12 (2021): 1386-1395. https://doi.org/10.1080/01430750.2019.1608860
[33] Quanwei, D. E. N. G., and L. I. N. Qizhao. "Numerical study of combustion in an HCCI fuelled with methane-hydrogen." Journal of University of Science and Technology of China 49, no. 6 (2019): 476. https://doi:10.3969/j.issn.0253-2778.2019.06.007
[34] Yu, Hanzhengnan, Xingyu Liang, and Gequn Shu. "Numerical study of the early injection parameters on wall wetting characteristics of an HCCI diesel engine using early injection strategy." International Journal of Automotive Technology 18 (2017): 759-768. https://doi.org/10.1007/s12239-017-0075-8
[35] Sharma, T. Karthikeya, G. Amba Prasad Rao, and K. Madhu Murthy. "Numerical investigations on HCCI engine with increased induction induced swirl and engine speed." Journal of Central South University 22 (2015): 3837-3848. https://doi.org/10.1007/s11771-015-2928-5
[36] Suryantoro, M. Taufiq, Bambang Sugiarto, and Fariz Mulyadi. "Growth and characterization of deposits in the combustion chamber of a diesel engine fueled with B50 and Indonesian biodiesel fuel (IBF)." Biofuel Research Journal 3, no. 4 (2016): 521-527. https://doi.org/10.18331/BRJ2016.3.4.6
[37] Bidita, B. S., A. R. Suraya, M. A. Shazed, MA Mohd Salleh, and A. Idris. "Preparation, characterization and engine performance of water in diesel nanoemulsions." Journal of the Energy Institute 89, no. 3 (2016): 354-365. https://doi.org/10.1016/j.joei.2015.03.004
[38] H. M. Tobib, "Experimental Investigation on Performance of Homogeneous Charge Compression Ignition Engine Fueled with Palm Oil Based Biodiesel," Universiti Putra Malaysia, 2019.
[39] Ansys, "Forte Theory Manual," *ANSYS Inc., USA*. 2021.
[40] Patel, Amar, Song-Charng Kong, and Rolf D. Reitz. Development and validation of a reduced reaction mechanism for HCCI engine simulations. No. 2004-01-0558. SAE Technical Paper, 2004. https://doi.org/10.4271/2004-01-0558
[41] Ganji, Prabhakara Rao, Rudra Nath Singh, V. R. K. Raju, and S. Srinivasa Rao. "Design of piston bowl geometry for better combustion in direct-injection compression ignition engine." Sādhanā 43 (2018): 1-9. https://doi.org/10.1007/s12046-018-0907-x

[42] Vaz, Marilia Gabriela J., Felipe Grossi L. Amorim, Jean Helder M. Ribeiro, Rudolf Huebner, and Ramon Molina Valle. Numerical analysis of the piston crown geometry influence on the tumble and squish in a single cylinder engine. No. 2014-36-0300. SAE Technical Paper, 2014. https://doi.org/10.4271/2014-36-0300

[43] Fujimoto, Masahiko, Kohei Iwai, Motoshi Kataoka, and Michihiko Tabata. "Effect of combustion chamber shape on tumble flow, squish-generated flow and burn rate." JSAE review 23, no. 3 (2002): 291-296. https://doi.org/10.1016/S0389-4304(02)00201-1

[44] Yakhot, Victor, and Steven A. Orszag. "Renormalization group analysis of turbulence. I. Basic theory." Journal of scientific computing 1, no. 1 (1986): 3-51. https://doi.org/10.1007/BF01061452

[45] Ansys, "ANSYS Chemkin-Pro Theory Manual." ANSYS Inc., USA, 2022.

[46] Mobasheri, Raouf, Abdel Aitouche, Zhijun Peng, and Xiang Li. "A numerical study of the effects of oxy-fuel combustion under homogeneous charge compression ignition regime." International Journal of Engine Research 23, no. 4 (2022): 649-660. https://doi.org/10.1177/1468087421993359

[47] Henein, Naeim A., A. Bhattacharyya, Jeremy Schipper, A. Kastury, and Walter Bryzik. Effect of injection pressure and swirl motion on diesel engine-out emissions in conventional and advanced combustion regimes. No. 2006-01-0076. SAE Technical Paper, 2006. https://doi.org/10.4271/2006-01-0076

[48] Kumar, Prashant, Ashok Darsigunta, B. Chandra Mouli, Vinod Kumar Sharma, Neeraj Sharma, and Anil Singh Yadav. "Analysis of intake swirl in a compression ignition engine at different intake valve lifts." Materials Today: Proceedings 47 (2021): 2869-2874. https://doi.org/10.1016/j.matpr.2021.03.663

[49] Bari, S., S. N. Hossain, and I. Saad. "A review on improving airflow characteristics inside the combustion chamber of CI engines to improve the performance with higher viscous biofuels." Fuel 264 (2020): 116769. https://doi.org/10.1016/j.fuel.2019.116769